Aerotecnica Missili & Spazio
https://doi.org/10.1007/s42496-024-00204-w

RESEARCH

A CFRP Passenger Floor Stanchion Underwent Dynamic Buckling Structural Testing

G. Di Mauro[1] · M. Guida[1] · F. Ricci[1] · L. Maio[1]

Received: 15 December 2023 / Revised: 4 February 2024 / Accepted: 14 February 2024

Abstract
The work focuses on the study of the structural behaviour of a composite floor beam in the cargo area of a commercial aircraft subjected to static and dynamic loads (typical of hard or crash landing). Experimental tests have been performed in the laboratories of the Dept. of Industrial Engineering (UniNA) jointly with the development of numerical models suitable to correctly simulate the phenomenon through the LS-DYNA software. The definition of a robust numerical model allowed to evaluate the possibility of buckling triggering. The test article was equipped with potting supports on both ends of the tested beam, filling the pots with epoxy resin toughened with glass fiber nanoparticles. This allowed to uniformly load the beam ends in compression and to carry out the tests loading the specimen statically and dynamically, to observe the differences in the behaviour of the beam under two different types of applied load. The comparison between the numerical and the experimental results shows that the dynamic buckling was triggered by a quantitatively smaller load than in the static case. On the other hand, it is observed this phenomenon to postpone the failure of the structure, due to the significantly higher displacement with respect to the quasi-static case to reach that condition.

Keywords Composite material · Transient analysis · Test validation · Dynamic buckling

1 Introduction

Buckling is an instability phenomenon that is common in "thin" structures (those with at least one relatively smaller dimension in comparison to the others). Buckling was formerly thought to be a totally static occurrence. The classic example is the Euler beam, in which a beam clamped at one end is axially compressed at the free end.

Depending on the applied load, the beam can return to the initial equilibrium configuration (stable equilibrium, below the critical compressive load), move to a new equilibrium condition different from the initial one but with certain constraints (indifferent equilibrium, at the critical compressive load), or move away from the initial equilibrium configuration indefinitely (unstable equilibrium, above the critical compressive load). The buckling load is the smallest load for which equilibrium is indifferent.

Buckling can, however, be produced by time-dependent loads. A demonstration to that is given in [1–3] where the application of a time-dependent axial stress to a beam has been investigated, causing lateral vibrations and eventually leading to instability.

Dynamic buckling is a relatively new phenomenon. One of the first researcher investigating dynamic buckling is Zizicas [4], who proposed a theoretical solution for a simply supported rectangular plate exposed to variable floor loads over time. A criterion that connected dynamic buckling to load duration was developed by Budiansky [5], Lindberg, and Florence [6] where the effect of a high-intensity, short-duration load was investigated.

In [7], results of dynamic buckling due to impulsive loads applied to thin-walled carbon-fiber reinforced plastic shell structures subjected to compressive axial loads are reported. The considered approach was based on the equations of motion, numerically solved using an explicit finite-element

✉ G. Di Mauro
gennaro.dimauro@unina.it

M. Guida
michele.guida@unina.it

F. Ricci
fabrizio.ricci@unina.it

L. Maio
dleandro.maio@unina.it

[1] Department of Industrial Engineering, University of Naples Federico II, Naples, Italy

Published online: 22 March 2024

code. It was shown that geometric imperfections as well as the duration of the loading period had a great influence on the dynamic buckling of the shells.

In [8–10], the relationship between dynamic and static buckling load has been pointed out, depending on several factors such as the duration of impact (i.e., duration of load application), the panel geometry (flat or curved panel), and also the presence of initial imperfections in the geometry. Particularly, for short-duration loads, the dynamic buckling load increases relative to the equivalent static buckling load. With increasing load duration, on the other hand, the dynamic critical load becomes much lower than the static one. Regarding the geometry, the dynamic buckling load increases relative to the static one as the curvature increases.

Other parameters influencing this phenomenon are the boundary conditions and the strain rate effects, investigated in [11] and [12], respectively.

In recent years, the dynamic buckling analysis has been extended also to stiffened panels. In [13], the dynamic buckling of simply supported stiffened panels under in-plane impact load was studied using the theory of large deflection. The influence of imperfection on dynamic responses of stiffened panels under in-plane impact was investigated in [14], finding the dynamic buckling to be sensitive to local imperfection, but not to overall ones. Also, in the case of stiffened panels, the boundary conditions play a fundamental role, as expected from the previous results. In detail, the effect of the constrained edge rotation on dynamic buckling of stiffened panels under uniaxial in-plane impact is investigated in [15]. Then, Yang et al. [16] showed that the influence of the rotation constraint around the unloaded edges on dynamic buckling was more significant than that around the loaded edges.

The definition of dynamic buckling is arbitrary, and consequently, there is still no unambiguous criterion for its determination, nor there are guidelines for the design of structures resistant to it. Budiansky and Hutchinson proposed a criterion that leads to a rational definition of dynamic instability [17]. A widely accepted definition of dynamic instability of imperfect structures states that instability occurs when a small increase in load intensity results in unlimited growth of deflections [18].

In this study, the structural behaviour of a composite floor beam has been explored. The aim is to conduct an experimental numerical investigation of the dynamic buckling phenomenology on a composite material beam. It was important to modify the test object to make sure that the experimental test was carried out correctly. In particular, both the stanchion ends were equipped with pottings, made out of steel pots filled with epoxy resin toughened by glass fiber nanoparticles to guarantee the compressive force to be applied symmetrically and uniformly over the entire beam cross-section. The resin was cured in the pots, at 60 °C temperature and 10% humidity.

The department laboratory's test equipment was used to conduct the experimental tests. On the other hand, the LS-DYNA software was used to numerically simulate the treated phenomena.

2 Case Study Description

The structure examined during this study was a beam belonging to the fuselage trunk lower section of a commercial aircraft, as showed in Fig. 1.

For the sake of completeness, the total length of the beam was 380 mm, also accounting for the connection areas with the frame and the floor truss of the considered fuselage section. The beam has been cut orthogonally with respect to the loading direction, to consider only its free length, the one in which the dynamic buckling phenomena can happen.

Fig. 1 Section of interest of the commercial aircraft fuselage trunk (left) with a focus on the test article (right) [19]

Therefore, the test article has a length of 315 mm and a cross-sectional area of 343.6 mm^2. Such a length of the beam also accounts of the terminal areas, covered by two rectangular pottings with a length of 25.40 mm. The pottings were needed to make sure that the experimental test was carried out correctly, with a uniformly distributed compressive force applied over the beam cross-section.

The test article and the numerical model, discretized in the LS-DYNA Finite-Element (FE) environment, are reported in Fig. 2.

The beam is transversely orthotropic, given its stacking sequence [−45; 45; 90; 45; −45; 0; 0; 0; 0; 0; −45; 45; 90; 45; −45]. The reference for the carbon-fiber plies orientation is the longitudinal axes, thus the direction of the applied compressive load.

The mechanical properties reported in Table 1 are referred to the single lamina of the composite material adopted for the beam manufacturing [19].

Table 1 Mechanical properties of the lamina [19]

Property	Value
ρ [g/cm^3]	1.6
th [mm]	0.186
E_{11} [MPa]	135,000
E_{22} [MPa]	8430
G_{12} [MPa]	4160
G_{13} [MPa]	4160
G_{23} [MPa]	3328
ν_{12}	0.26
Xt [MPa]	2257
Xc [MPa]	800
Yt [MPa]	75
Yc [MPa]	171
Sc [MPa]	85

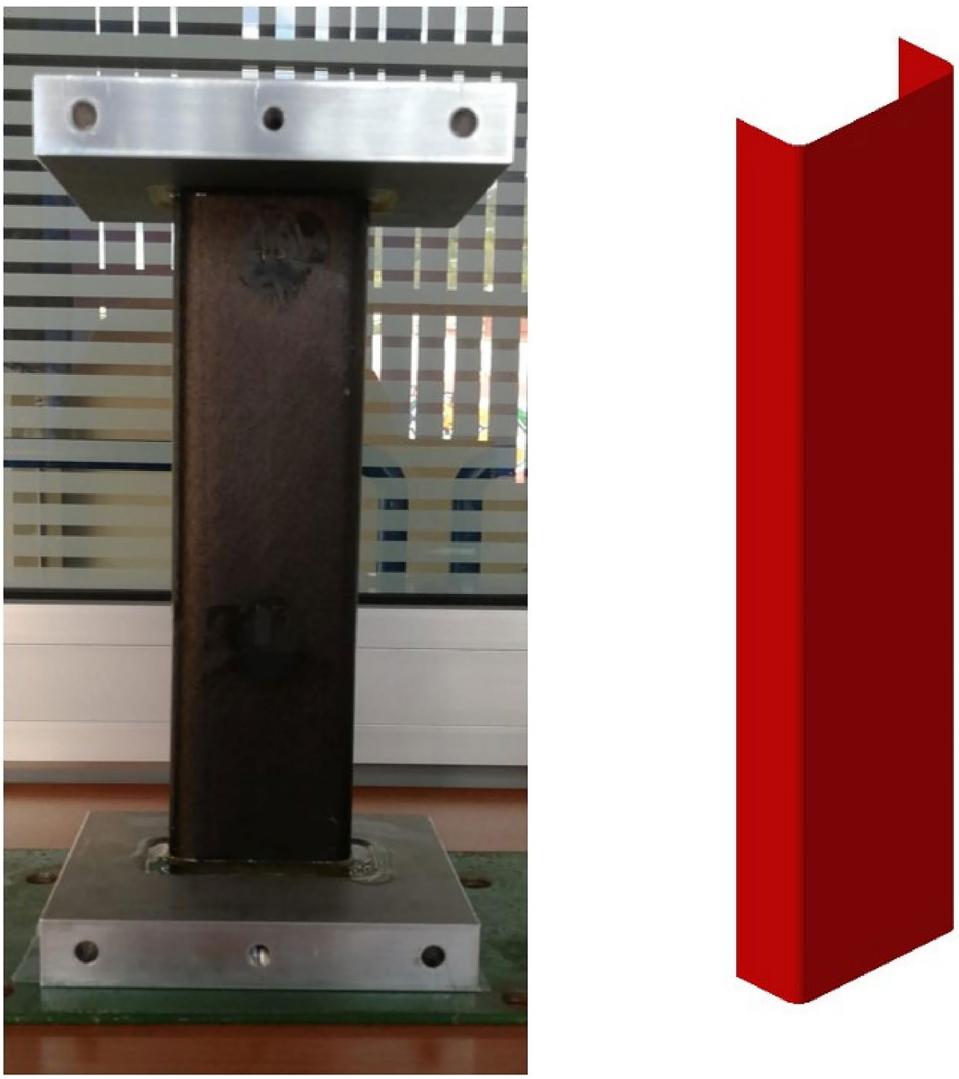

Fig. 2 Test article (left) and isometric view for the numerical model adopted to discretize the test article (right)

Concerning the numerical model, to find the optimal balance between computational costs and the correctness of the findings in terms of expected stiffness, a preliminary mesh convergence study has been performed. As a result, several quasi-static linear studies with varied in-plane element sizes and through-the-thickness configurations have been carried out.

In detail, the stanchion model was realized by considering shell elements in the middle plane of its cross-sectional area. Three different discretization strategies have been adopted, differing in the element size: coarser (8 mm), moderate (4 mm), and finer (2 mm). The investigated meshing strategies are illustrated in Fig. 3, where a detailed view of the shell elements on the middle plane of the stanchion cross-sectional area is shown for each of them.

Furthermore, for each of the assumed meshing strategies, three different through-the-thickness configurations have been considered. Thus, nine distinct model in total has been examined. Regarding that, the discriminating parameter between the three adopted configurations is the number of integration points, which was set to be 16 for the first configuration. The second and the third configurations have been obtained by considering, respectively, 4 and 2 integration points in through-the-thickness direction of shell elements.

Noteworthy is that in the first configuration, given the number of integration points, it has been possible to reproduce exactly the stanchion material stacking sequence. On the other hand, for the second configuration, the cross-sectional area was divided into three areas. In this way, given the stacking sequence, it has been possible to ideally divide the laminate in three sub-laminates: the central one containing only 0° plies and the outer ones equal to each other.

In particular, the Classic Lamination Theory (CLT) has been applied to get the outer sub-laminate properties, reported in Table 2. Clearly, it was not necessary to get the properties of the central sub-laminate, since containing only 0° plies. Thus, in this case, the lamina-level properties have considered, only changing the thickness value (th = 0.93).

Following the same approach, also the third configuration has been realized; in this case, the CLT has been applied to get the mechanical properties for all the stacking sequence. In particular, the laminate properties are reported in Table 3.

For a better understanding, a schematization of the investigated through-the-thickness configurations is presented in Fig. 4.

Table 2 Mechanical properties of the outer sub-laminate

Property	Value
ρ [g/cm^3]	1.6
th [mm]	0.93
E_{11} [MPa]	22,674
E_{22} [MPa]	39,437
E_{33} [MPa]	8430
G_{12} [MPa]	28,759
G_{13} [MPa]	28,759
G_{23} [MPa]	3328
ν_{12}	0.44
ν_{13}	0.3
ν_{23}	0.3

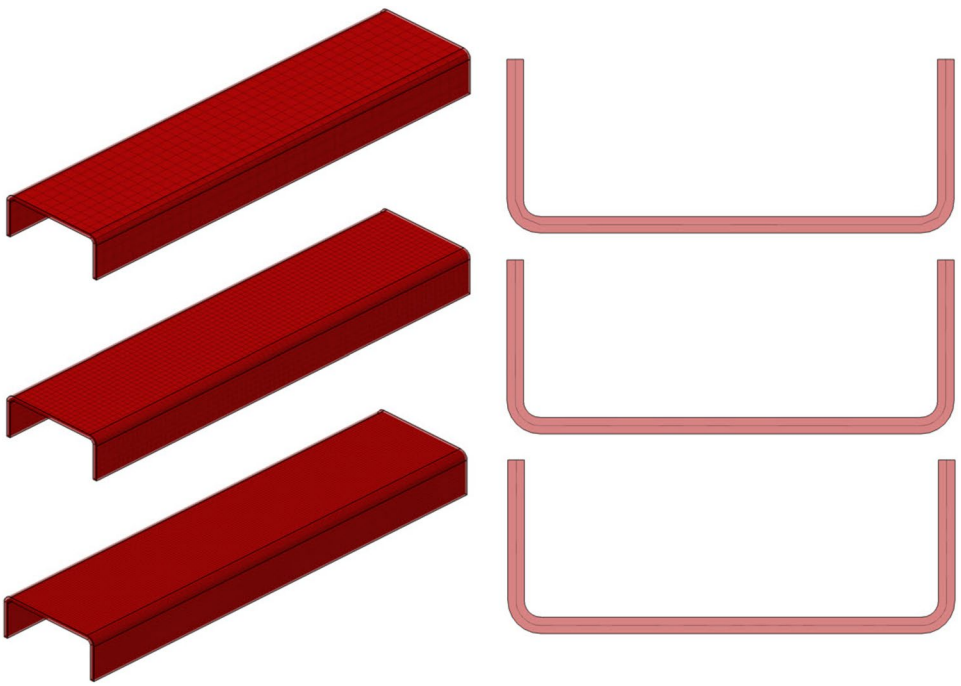

Fig. 3 Investigated meshing strategies for the test article: coarser (top), moderate (middle), and finer (bottom). In particular, for each configuration is shown both the isometric view of the numerical model (left) and a detailed view of the shell elements on the middle plane of the stanchion cross-sectional area (right)

Table 3 Mechanical properties of the laminate

Property	Value
ρ [g/cm^3]	1.6
th [mm]	2.79
E_{11} [MPa]	60,267
E_{22} [MPa]	37,845
E_{33} [MPa]	8430
G_{12} [MPa]	20,559
G_{13} [MPa]	20,559
G_{23} [MPa]	3328
ν_{12}	0.43
ν_{13}	0.3
ν_{23}	0.3

The best ratio between results effectiveness and computational cost was provided by the model characterized by a moderate size mesh, with 16 integration points through the thickness.

The adopted material card was the *MAT_LAMINATED_COMPOSITE_FABRIC, fulfilled with the parameters reported in the Tables.

The model boundary conditions have been set compatibly with the experimental test conditions. The beam has one base fixed (the top surface), while the other is free to move along the longitudinal axis. Then, constraints must be added to simulate the mechanical behaviour of the two pottings, which were decided to not discretize. Specifically, pottings were introduced to impose compression-only stresses at the end of the beam to prevent it from buckling in these areas. Constraints were, therefore, applied to lock the degrees of freedom related to the three rotations and in-plane translations for the nodes in the pottings areas. For the sake of clarity, the described boundary conditions are shown in Fig. 5, highlighting the node sets on which they have been applied.

The loading condition is realized by adding to the model a rigid frame, needed to simulate, together with the boundary conditions, the experimental test set-up. In particular, the compressive load to be applied on the stanchion model is realized by a displacement curve imposed on the rigid frame, for it to move along the longitudinal axis. The numerical model of the rigid frame is realized by solid elements, with the same size as the stanchion ones. This choice is justified by the aim of obtaining a stable contact between the rigid frame itself and the bottom surface of the beam, through which the load is transferred. Noteworthy is the simplification introduced in the discretization of the frame itself, which is not subject to deformation since rigid, as it is experimentally expected. For the sake of clarity, the complete numerical model, together with a focus on the rigid frame, is shown in Fig. 6.

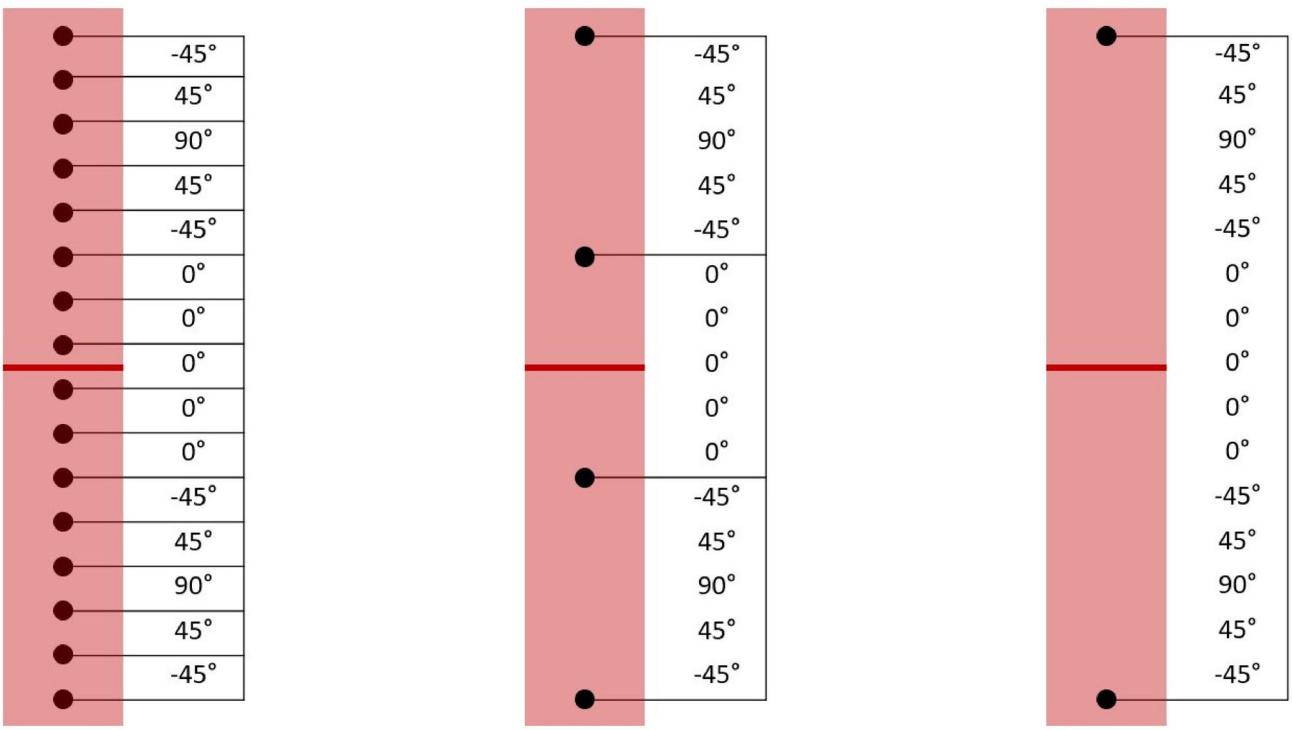

Fig. 4 Investigated through-the-thickness configurations: 16 (left), 4 (middle), and 2 (right) integration points are considered

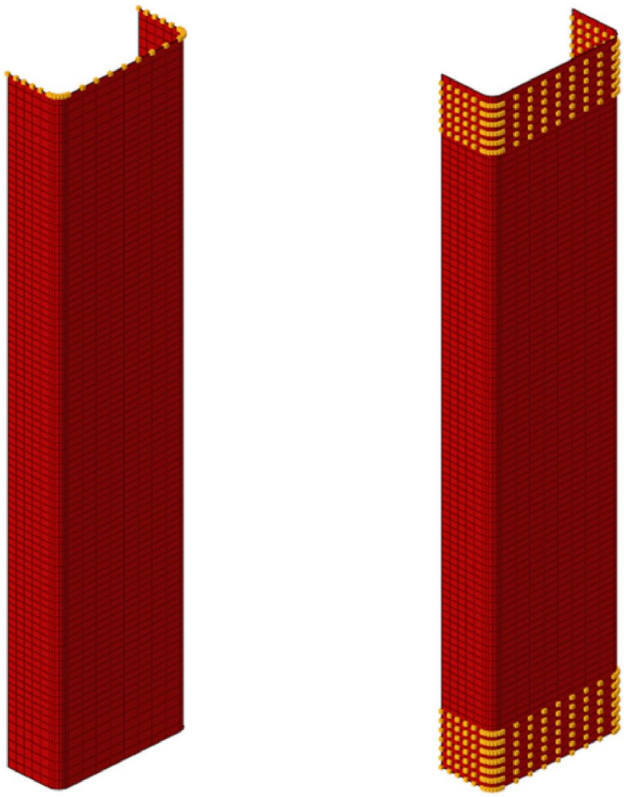

Fig. 5 Test article boundary conditions: highlighted is the node set for fixing the top surface (left) and the node set for simulating the presence of the two pottings (right)

3 Results

The numerical model has been validated by comparison with the experimental test results reported in [19]. In particular, a quasi-static analysis has been considered up to the ultimate failure. In Fig. 7, the load curve as a function of the displacement is shown, both for the numerical simulation and the experimental test.

According to these experimental results, the failure load was 103.7 KN, and up to the failure load, there were no buckling events, as also confirmed numerically. Table 4 reports the failure displacements and loads, showing a good agreement.

Then, for a further validation of the numerical model, a new compressive experimental test was performed, without taking the failure into account, to confirm the linear deformation of the stanchion. Figure 8 shows the adopted experimental test set-up. The department laboratory's test equipment was used to conduct the experimental tests. It is characterized by two rigid steel blocks, the top and the bottom ones, both connected to hydraulic pistons. The top plate is locked after the sample positioning, while the bottom one is free to move along the longitudinal direction to apply the desired load, compatibly with the assigned displacement curve.

Figure 9 shows the good agreement of the load curve as a function of the displacement between the numerically predicted solution and the outcomes of the new experimental campaign.

Once the numerical model was validated, with respect to experimental data obtained under quasi-static conditions, the dynamic simulation was executed by modifying the rigid frame speed, which was set to 100 mm/s. To investigate how the dynamic buckling phenomenon would have occurred, the approach expressed in [19] has been followed, where a decrease in stiffness was evaluated as a warning of buckling approaching. In Fig. 10, it is shown how the stanchion stiffness undergoes a sudden drop due to dynamic buckling. In

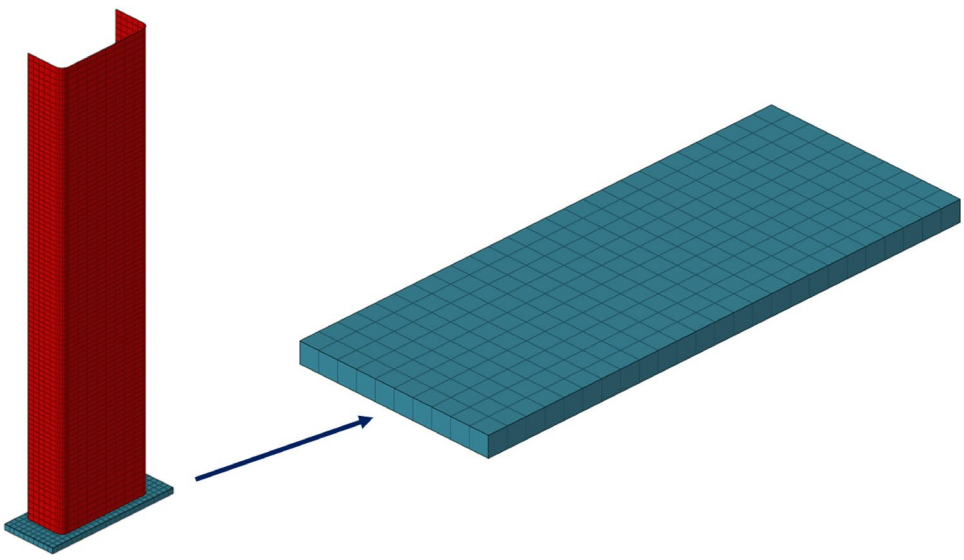

Fig. 6 Numerical model of the test article with a focus on the rigid frame

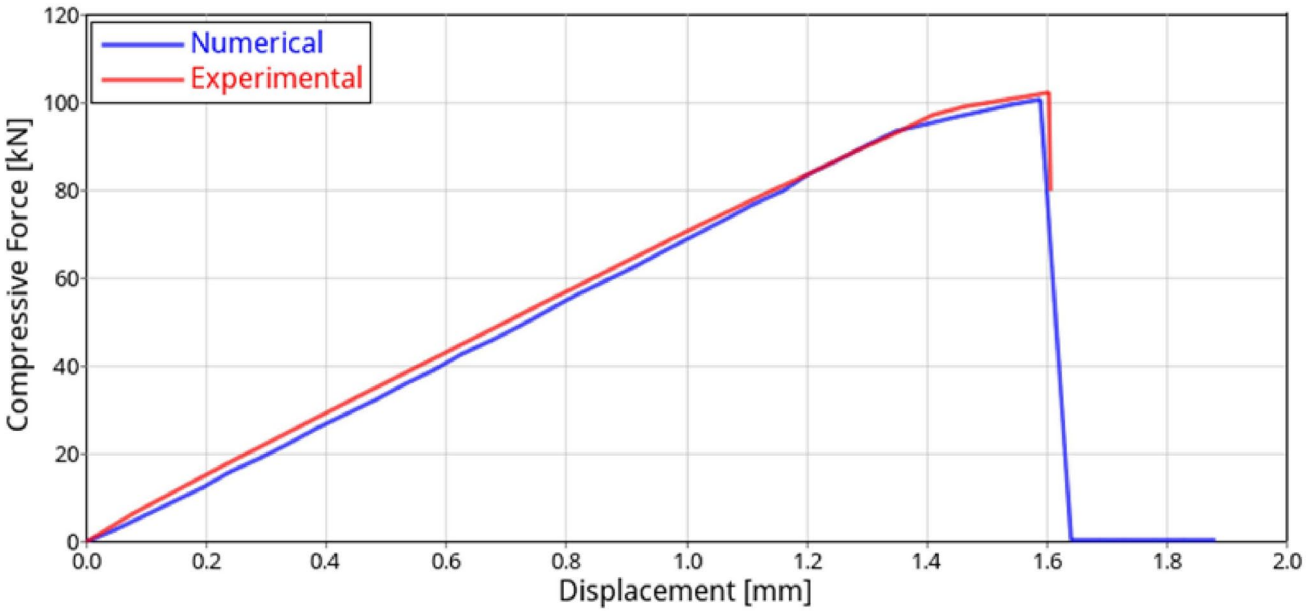

Fig. 7 Numerical–experimental comparison for quasi-static load–displacement curves [19]

Table 4 Numerical–experimental comparison for quasi-static load application: failure displacement and failure load

	Failure Displacement	Failure Load
Numerical	1.59 mm	100.8 kN
Experimental	1.6 mm	103.7 kN
Error	0.6%	2.9%

detail, the timeframe in which stiffness undergoes a significant decrease is highlighted. Thus, from comparison with the load curve as a function of the displacement (reported in Fig. 11), it is clearly visible that the phenomenon of dynamic buckling instability occurs after 0.014 s with a bucking load equal to 90 kN.

Figure 12 shows the out-of-plane displacements evolution along the load–displacement curve for the dynamic simulation. In detail, these displacements are nearly null up to the buckling load. Once that value is exceeded, the force–displacement curve exhibits a plateau, which coincides with the occurrence and progressive growth of out-of-plane displacements. This phenomenon makes the structure more efficient in terms of energy absorption, since a greater quantity of the stanchion surface is called to collaborate. In particular, some of the mechanical energy resulting from the application of the load is lost due to the deformation that took place after the beam protruded from its axis. This is substantially different from what happens in the case the load is applied quasi-statically. Here, the displacements are localized in the failure area, since the load–displacement curve maintains its linear trend, until it undergoes a sudden drop after the critical load is reached.

Fig. 8 Adopted experimental test set-up

Finally, the model robustness is highlighted in Fig. 13, in which it is shown the failure location is well predicted to be in the middle area of the stanchion.

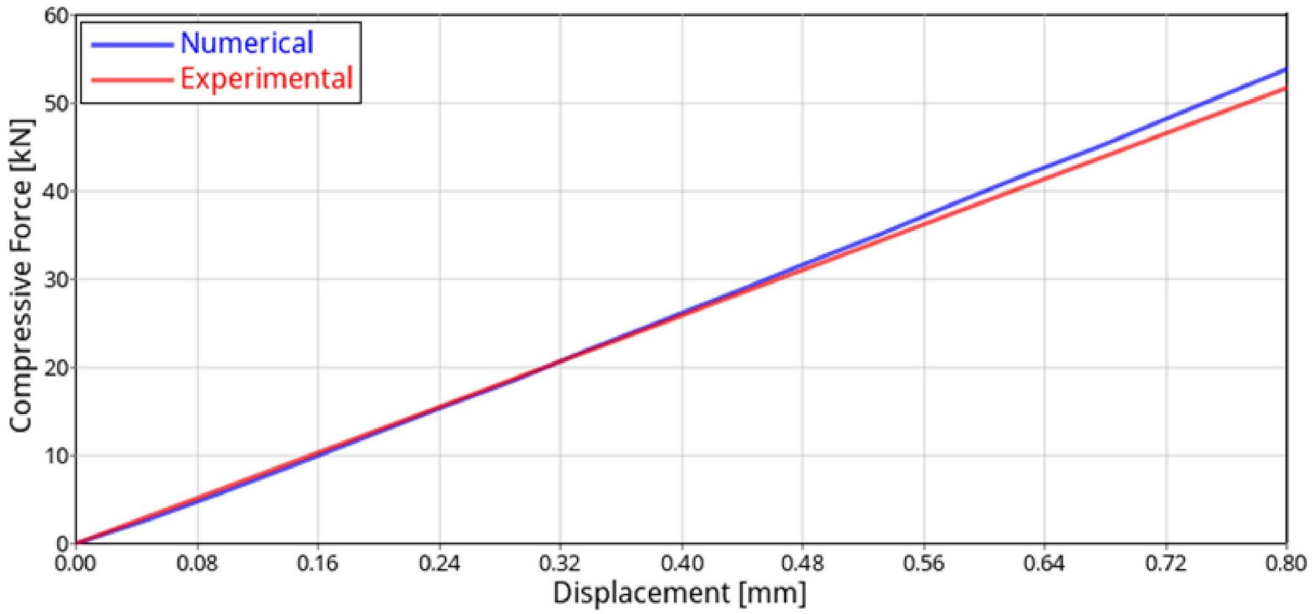

Fig. 9 Numerical–experimental comparison for quasi-static load–displacement curves for linear deformation confirmation

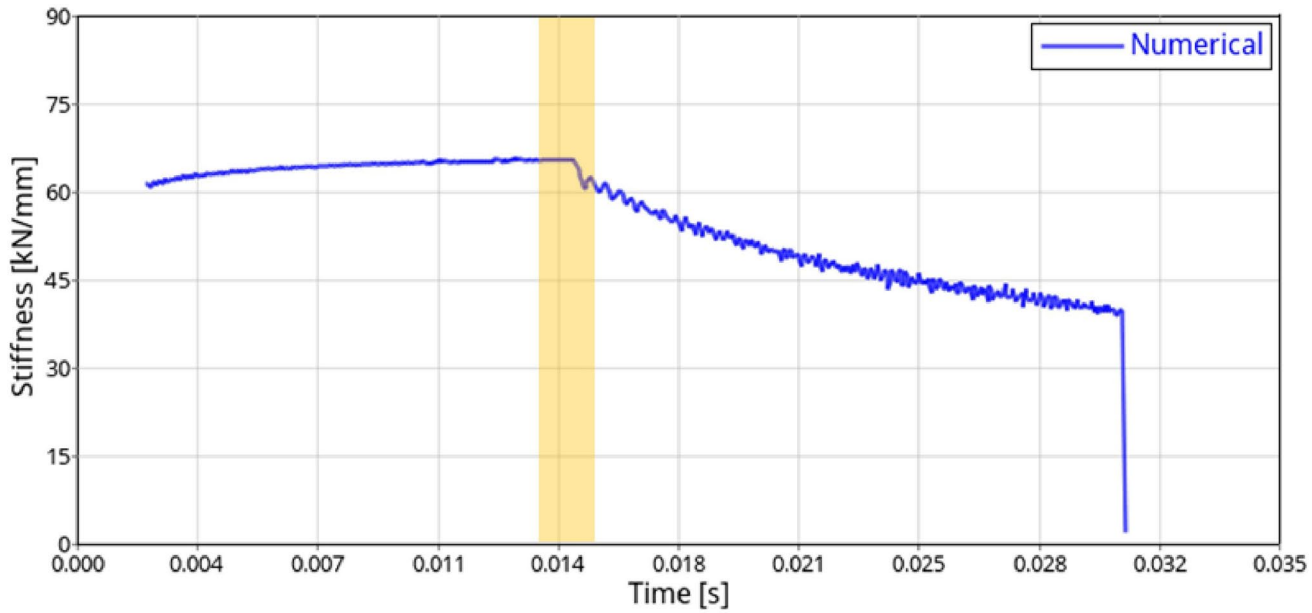

Fig. 10 Dynamic simulation: stiffness variation due to dynamic buckling

4 Conclusions

The work focuses on the study of the structural behaviour of a composite floor beam in the cargo area of a commercial aircraft subjected to static and dynamic loads (typical of hard or crash landing). The research state of the art on the relevant topic of dynamic buckling is provided. The performed activity is fully detailed, both from experimental and numerical point of view.

In detail, once the numerical model has been validated with respect to experimental data obtained under quasi-static conditions, the dynamic bucking phenomena are numerically investigated. It is clear from an examination of the findings that for composite material structures, the

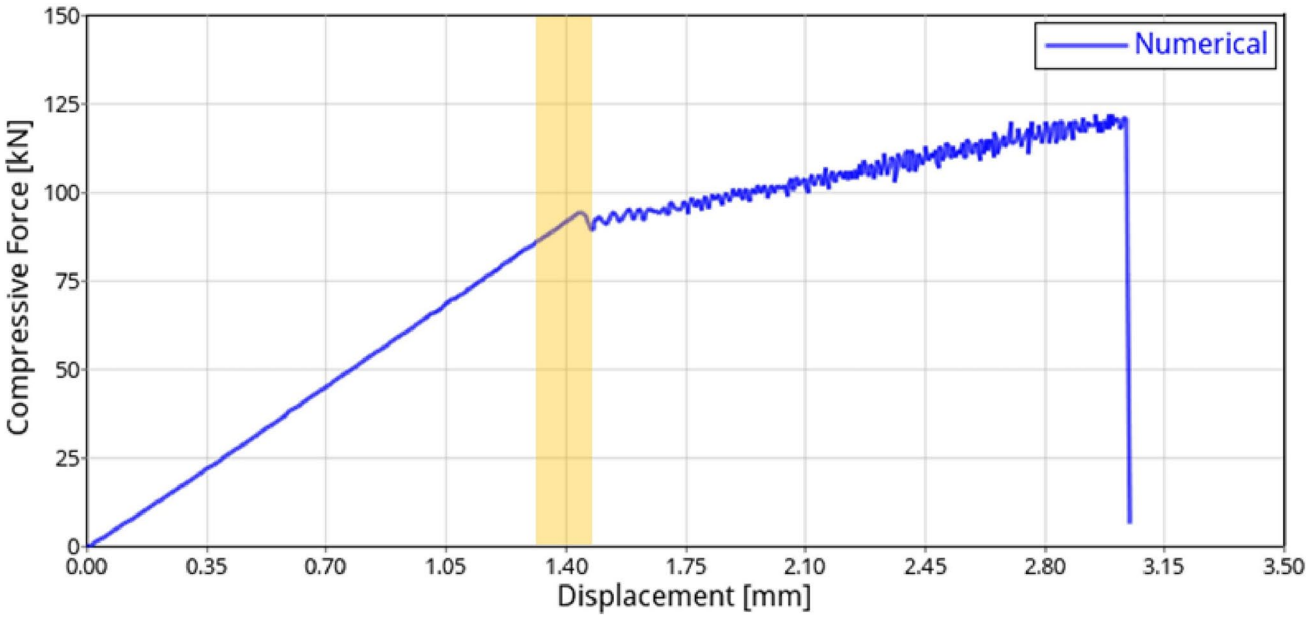

Fig. 11 Dynamic simulation: load–displacement curve

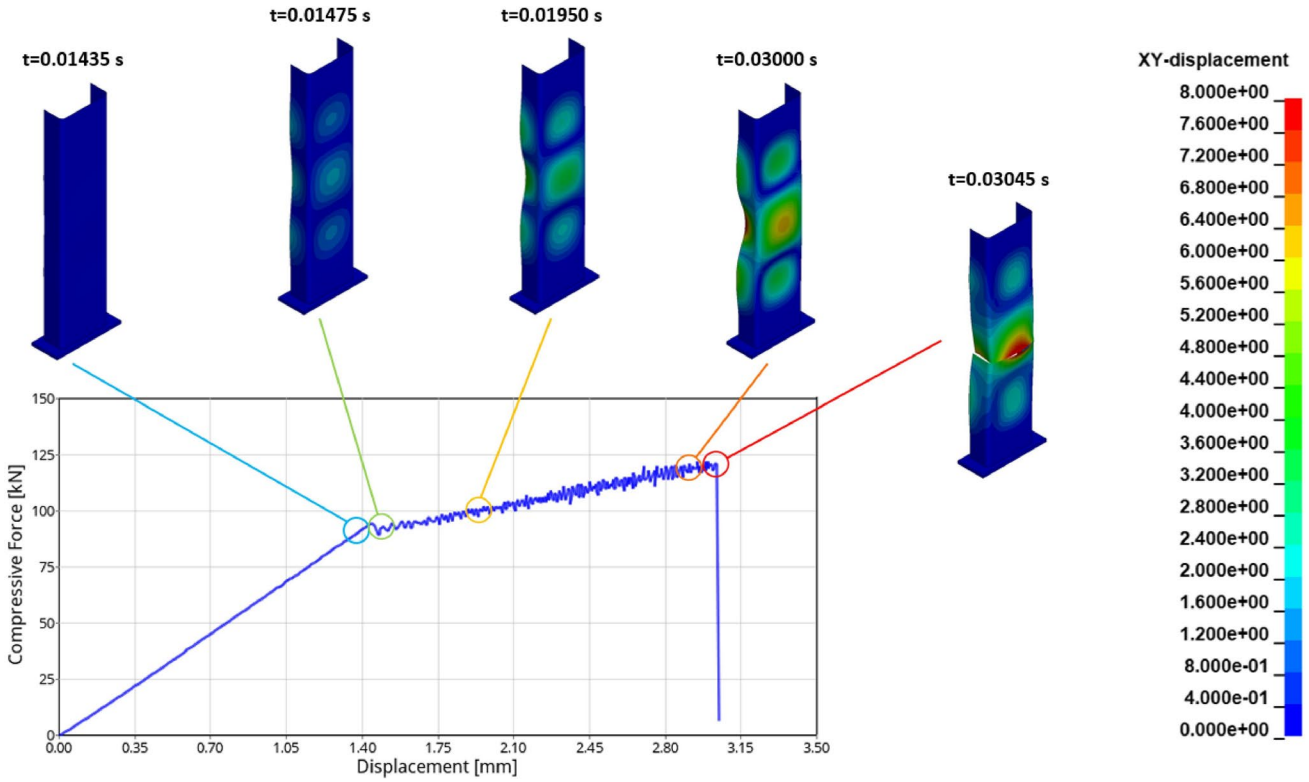

Fig. 12 Out-of-plane displacement evolution within dynamic simulation

buckling load in a dynamic compression test assumes a lower value than the critical load in a quasi-static compression test. On the other hand, a larger displacement with respect to the quasi-static compression test is required to cause the collapse of the structure, making it more efficient in terms of energy absorption. Regarding that, it is shown how the structure operates in post-buckling

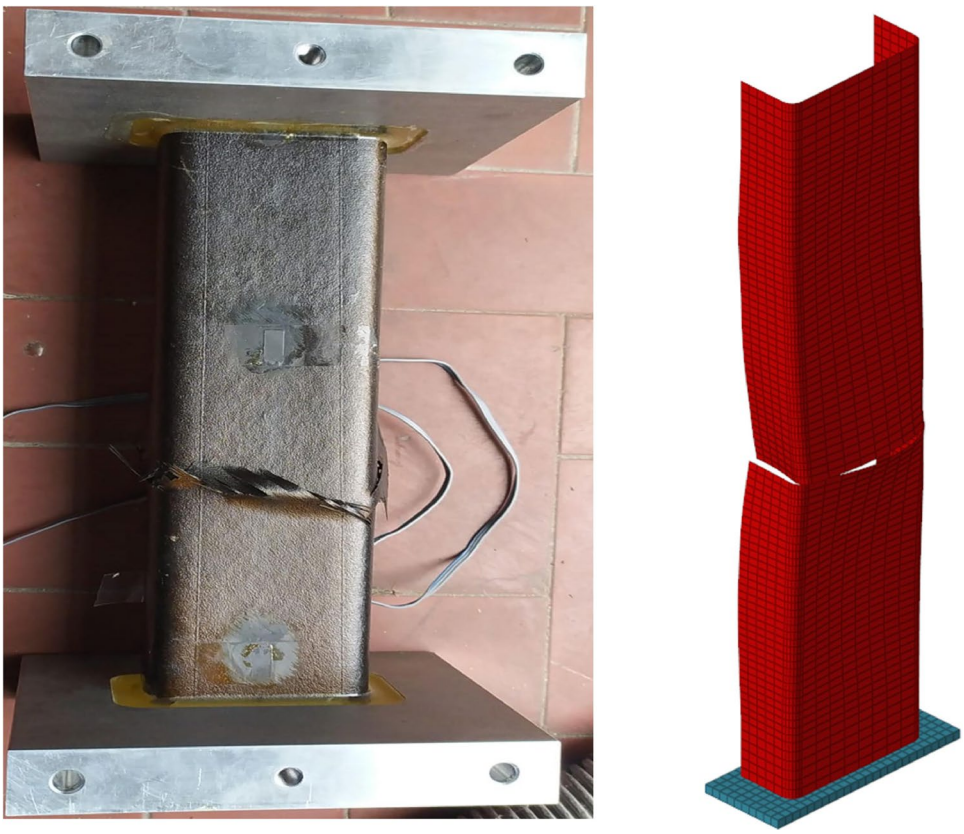

Fig. 13 Failure location for dynamic test (left) and simulation (right)

conditions, absorbing by deformation the mechanical energy due to the load application.

Acknowledgements The authors declare that they have no conflict of interest to disclose.

Author Contributions G. Di Mauro wrote the main manuscript; F. Ricci, M. Guida, L. Maio revised it for important intellectual content; M. Guida approved the version to be published. All authors reviewed the manuscript.

Funding Open access funding provided by Università degli Studi di Napoli Federico II within the CRUI-CARE Agreement.

Data Availability No datasets were generated or analysed during the current study.

Declarations

Conflict of Interest The authors declare no competing interests.

References

1. Amabili, M., Païdoussis, M.P.: Review of studies on geometrically nonlinear vibrations and dynamics of circular cylindrical shells and panels, with and without fluid-structure interaction. Appl. Mech. Rev. **56**(4), 349–381 (2003)
2. Alijani, F., Amabili, M.: Non-linear vibrations of shells: A literature review from 2003 to 2013. Int. J. Non-Linear Mech. **58**, 233–257 (2014)
3. Kubiak, T.: Static and dynamic buckling of thin-walled plate structures, pp. 27–47. Springer International Publishing, Heidelberg (2013)
4. Zizicas, G.A.: Dynamic buckling of thin elastic plates. Trans. Am. Soc. Mech. Eng. **74**(7), 1257–1266 (1952)
5. Budiansky, B.: Axisymmetric dynamic buckling of clamped shallow spherical shells. NASA TN **1510**, 597–606 (1962)
6. Lindberg, H. E., & Florence, A. L. (1987). Dynamic pulse buckling: theory and experiment (Vol. 12). Springer Science & Business Media.
7. Bisagni, C.: Dynamic buckling of fiber composite shells under impulsive axial compression. Thin-walled Struct. **43**(3), 499–514 (2005)

8. Kuzkin, V. A. (2015). Structural model for the dynamic buckling of a column under constant rate compression. arXiv preprint arXiv:1506.00427.
9. Petry, D., Fahlbusch, G.: Dynamic buckling of thin isotropic plates subjected to in-plane impact. Thin-Walled Struct. **38**(3), 267–283 (2000)
10. Zheng, Z., Farid, T.: Numerical studies on dynamic pulse buckling composite laminated beams subjected to an axial impact pulse. Compos. Struct. **56**(3), 269–277 (2002)
11. Azarboni, H.R., Darvizeh, M., Darvizeh, A., Ansari, R.: Nonlinear dynamic buckling of imperfect rectangular plates with different boundary conditions subjected to various pulse functions using the Galerkin method. Thin-Walled Struct. **94**, 577–584 (2015)
12. Yang, B., Soares, C.G., Wang, D.Y.: Dynamic ultimate compressive strength of simply supported rectangular plates under impact loading. Mar. Struct. **66**, 258–271 (2019)
13. Zhang, T., Liu, T.G., Zhao, Y., Luo, J.Z.: Nonlinear dynamic buckling of stiffened plates under in-plane impact load. J. Zhejiang University-SCIENCE A **5**, 609–617 (2004)
14. Ji, Z.H., Wang, D.Y.: Influence of load shape on dynamic response of cross-stiffened deck subjected to in-plane impact. Thin-Walled Struct. **82**, 212–220 (2014)
15. Yang, B., Wang, D.Y.: Dynamic buckling of stiffened plates with elastically restrained edges under in-plane impact loading. Thin-Walled Struct. **107**, 427–442 (2016)
16. Yang, B., Li, Y., Fu, K.: In-plane impact-induced elastic buckling behaviour of rectangular transversally isotropic stiffened plates with all edges elastically restrained against rotation. Int. J. Mech. Sci. **174**, 105478 (2020)
17. Hutchinson, W.J., Budiansky, B.: Dynamic buckling estimates. AIAA J. **4**(3), 525–530 (1966)
18. Ekstrom, R.E.: Dynamic buckling of a rectangular orthotropic plate. AIAA J. **11**(12), 1655–1659 (1973)
19. Sellitto, A., Di Caprio, F., Guida, M., Saputo, S., Riccio, A.: Dynamic pulse buckling of composite stanchions in the subcargo floor area of a civil regional aircraft. Materials **13**(16), 3594 (2020)